First principle calculations of the k-Fe3AlC perovskite and ironealuminium intermetallics

Damien Connétable, Philippe Maugis

First principle calculations of the κ-Fe_3AlC perovskite and iron−aluminium intermetallics

D. Connétable [a,*], P. Maugis [a,b]

[a] *CIRIMAT CNRS/UPS/INPT − ENSIACET, 118 route de Narbonne, 31077 Toulouse, France*
[b] *Arcelor Research, Voie Romaine, 57283 Maizières-lès-Metz, France*

Abstract

We present first principle calculations of the structural, electronic, magnetic, vibrational and elastic properties of the κ-Fe_3AlC perovskite, within the *ab initio* formalisms of the Density Functional Theory (DFT) and the linear response theory of the DFT. These properties are compared with those of the intermetallic Fe_3Al-$L1_2$ isostructural phase of κ, permitting to interpret the role of the carbon element. We also discuss the influence of the spin effects (GGA and SGGA approaches) on the vibrational properties of some Fe−Al intermetallics.

Keywords: E. Ab initio calculations; A. Iron aluminides, based on Fe_3Al; B. Elastic properties; E. Electronic structure, calculation

1. Introduction

It has been reported that aluminium-alloyed steels can be hardened by a dispersion of κ-Fe_3AlC carbides (see Refs [1−3]). The microstructures of such steels have been investigated in detail [4−6]. To control the precipitation microstructures of steels and also to master the carburising process of Fe−Al alloys, it is necessary to rely on the thermodynamical properties of the iron-rich phases in the Fe−Al−C system, and to know the fundamental properties of these phases. However, few and contradictory experimental and theoretical information are present in the literature about the κ carbide.

The κ phase is associated to the Fe_3AlC formula, with the *Strukturbericht Designation* $E2_1$ (a perovskite-type structure). This carbide is based on the fcc ordered structure Fe_3Al-$L1_2$ where the iron atoms are located in the center of each face, and the aluminium atoms sit on the corners of the cube (see Fig. 1). The carbon atom occupies the central octahedral interstitial position formed by the six iron atoms as first nearest neighbors. Due to the structural similarity between Fe_3Al-$L1_2$ and Fe_3AlC-$E2_1$, their properties will be compared in this paper.

The stoichiometry Fe_3AlC has, in fact, never been observed. Experimentally, the stoichiometry proposed for κ is $Fe_{4-y}Al_yC_x$ where $0.8 < y < 1.2$ and $0 < x < 1$ [7]. Results indicate that the composition of the different synthesized compounds is probably close to $Fe_3AlC_{x=1/2}$ [8,9]. In addition, the experimental magnetic nature of the compound (ferro- or non-magnetic) is not yet well established. Since the investigations of Morral (1934) [12], it has been stated several times that the kappa phase is ferromagnetic. The given Curie temperature values would lie between 125 [13] and 290 °C [14]. However, recent investigations of Parker et al. [15] indicate that the κ phase might not be magnetic. Later investigations of Andryushchenko et al. [7] seem to confirm these observations. These authors have observed that the distribution of aluminium on the corners of the cube and of iron on the faces of the cube is apparently not perfect. Antisites' defects (aluminium atoms on iron sites and reciprocally iron on aluminium sites) seem to be at the origin of the reduced magnetic moment.

Partial information have been published relating to the formation energy of the κ phase: Palm and Inden [8] have

* Corresponding author.
E-mail address: Damien.Connetable@ensiacet.fr (D. Connétable).

doi:10.1016/j.intermet.2007.09.011

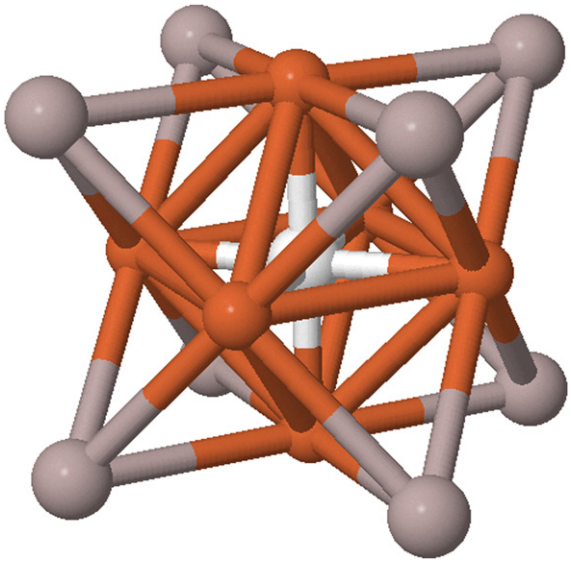

Fig. 1. Conventional cell of the κ-Fe_3AlC carbide. We have represented in white the carbon atom in octahedral position, in grey the aluminium atoms and in dark-grey the iron atoms.

investigated experimentally specific Gibb's isotherms of the Fe−Al−C system. Ohtani et al. [10] have recently published a Fe−Al−C phase diagram based on *ab initio* calculations within an all electron approach, and Maugis et al. [11] have discussed the relative stability of various phases in aluminium-containing steels, through *ab initio* calculations using the *VASP* package. However, published theoretical results are not well stated because of their dispersions, and no discussion on the electronic and vibrational properties has been clearly proposed.

Then, before exploring the non-stoichiometric κ phase [16], we propose to discuss here the ordered stoichiometric phase and present its intrinsic properties, taking into account or not the spin effects. We present also in this paper first principle calculations of the structural, magnetic, electronic, vibrational and elastic properties of the κ-Fe_3AlC carbide, and compare them to other Fe−Al intermetallics. We present consequently first principle calculations of the Fe_3Al-$L1_2$ phase and discuss those of the Fe_3Al-$D0_3$ phase − which are systems largely discussed by Lechermann and co-workers [17−20] − and also the FeAl-B2 system. Our results using SGGA and GGA functionals allow us to discuss their influence in Fe−Al systems.

2. Computational details

Our *ab initio* calculations have been done within the Density Functional Theory (DFT) developed by Hohenberg and Kohn [21,22]. The Perdew−Burke−Ernzerhof [23] (PBE) generalized gradient approximation (GGA) for the exchange and correlation functional in its spin polarized version was used.

Calculations have been done using the Quantum-*ESPRESSO* package [24] which is a self-consistent pseudo-potential code based on numerical plane wave as the basis set for decomposition of the one-electron wave functions. Ultrasoft pseudo-potentials [25] have been generated according to a modified Rappe−Rabe−Kaxiras−Joannopoulos (RRKJ) scheme following the method of Ref. [26]. For structure optimization, the Brillouin zone (BZ) was sampled by a $15 \times 15 \times 15$ Monkhorst and Pack grid [27]. The charge density was calculated on a real-space grid with a 50 Ryd energy cut-off, and the augmentation charges are expanded up to 600 Ryd. For the calculation of the electronic density of states and the formation energy, we have adopted a finest $30 \times 30 \times 30$ grid with a higher energy cut-off (60 Ryd).

All systems have been fully relaxed with respect to the atomic position and the unit cell size. To evaluate the bulk modulus, different unit cell volumes were performed, and the results were fitted by a Murnaghan equation of state [28].

The phonon properties were calculated at the equilibrium lattice using the linear response theory applied to the DFT as proposed by Baroni et al. [29,30], in its implemented version in the *ESPRESSO* package. In the harmonic approximation, dynamical matrices are derived via the linear response of the electronic subsystem. In order to generate the force constant matrices and carry out the inverse Fourier transformation we used **q** points from the $4 \times 4 \times 4$ mesh, with a $15 \times 15 \times 15$ **k** grid mesh with 50 Ryd of energy cut-off. Our calculations of the density of states were then performed using the tetrahedron method (with a $30 \times 30 \times 30$ mesh).

From the vibrational density of states we have evaluated the vibrational part of the free energy F_{vib} and the heat capacity C_v, from the following equations:

$$F_{\mathrm{vib}}(T) = k_{\mathrm{B}}T \sum_{\mathbf{q},\nu} \ln\left(2\sinh\left(\frac{\hbar\omega_{\mathbf{q},\nu}}{k_{\mathrm{B}}T}\right)\right) \tag{1}$$

$$C_v(T) = -T\frac{\partial^2 F_{\mathrm{vib}}}{\partial T^2}\bigg|_V = -k_{\mathrm{B}} \sum_{\mathbf{q},\nu} \left(\frac{\hbar\omega_{\mathbf{q},\nu}}{2k_{\mathrm{B}}T}\right)^2 \frac{1}{\sinh^2\left(\frac{\hbar\omega_{\mathbf{q},\nu}}{2k_{\mathrm{B}}T}\right)} \tag{2}$$

3. Results and discussion

3.1. Structural and cohesive properties

We present, first, *ab initio* calculations of the pure elements in their stable form, which are needed for the evaluation of the formation energy of the compounds formed from these elements, and to validate our pseudo-potentials. The results of the calculations of the bcc ferromagnetic iron, the fcc aluminium and the diamond carbon are given in Table 1. The lattice parameters and the bulk modulus lie within, respectively, 1% and ∼5% of the literature data measurements at room temperature. The magnetism of the bcc iron is found slightly higher (2.4 μ_{B}) in comparison with the experimental value (2.2 μ_{B}). This result is nevertheless in agreement with results found in the theoretical literature (see in particular Ref. [31]). In the following, we will not present the electronic and vibrational properties for these well-known reference phases, however, we have checked that our pseudo-potential approach reproduces

Table 1
The calculated and experimental lattice parameters, the volume V of the unit cell (in Å^3/at.), the formation energy E_f per atom (in meV/at.), the magnetic moment (in Bohr's magneton per iron atom), and the bulk modulus B_o (in GPa) ($sp \equiv$ spin polarized, and $np \equiv$ without spin effects)

	a_o (Å)	a_o^{exp} (Å)	V (Å^3/at.)	E_f (meV/at.)	μ_B/(at.Fe)	B_o	B_o^{exp}
C	3.57	3.57 [34]	5.7	–	–	431	445 [34]
Al-fcc	4.05	4.05 [34]	16.6	–	–	77	72 [34]
Fe-bcc	2.86	2.87 [37]	11.8	–	2.4 (2.29 [38])	171	168 [34]
FeAl-B2 (*sp*)	2.87		11.8	−277.0	0.36 (0.0 [39])	172	152 [52]
FeAl-B2 (*np*)	2.86	2.909 [35]	11.7	−253.0	–	179	–
Fe_3Al-$D0_3$	5.76	5.79 [41]	11.9	−185.3	2.1 (1.86 [42])	159	144 [35]
Fe_3Al-$L1_2$ (*sp*)	3.65		12.1	−199.2	2.3	185	–
Fe_3Al-$L1_2$ (*np*)	3.55		11.2	+206.7	–	210	–
Fe_3AlC-$E2_1$ (*sp*)	3.75	3.78 [8,40,43]	10.6	−134.2	1.1	215	–
Fe_3AlC-$E2_1$ (*np*)	3.73		10.3	−105.5	–	241	–

experimental data with a minimal error (less than 2%) using the SGGA−PBE functional (see Refs. [31−33]).

We report too, for information, results of two other systems not directly discussed in the following but useful to understand the Fe−Al−C system: FeAl-B2 and Fe_3Al-$D0_3$ intermetallics.

(a) *FeAl-B2*: Concerning the ordered compound FeAl-B2, we find a lattice parameter slightly smaller than the experimental value [35] (either with or without spin effects, see Table 1). Simulations incorporating or not the spin effects are in agreement with the calorimetry values (−249 to −419 meV/at. See Ref. [36] and references therein). However, as well described in the literature (see Ref. [20] and references therein), simulations indicate that the magnetic ground state is ferromagnetic with a magnetic moment of 0.36 μ_B/at.Fe, which is in contradiction with the experimental evidence that the perfect FeAl-B2 compound does not exhibit a macroscopic magnetic moment. Nevertheless, as we will see later, a simulation without spin polarization provides better results on the vibrational properties than with spin polarized for this system.

(b) *Fe_3Al-$D0_3$*: Our results about the Fe_3Al-$D0_3$ system agree with those presented by Lechermann et al. [18,19,44] and by Maugis [11]. The theoretical lattice parameter and bulk modulus reproduce correctly the experimental values. The ground state is found to be ferromagnetic, with a magnetic moment which is slightly overestimated compared to the experimental value, as for previous systems (Fe-bcc and FeAl-B2), and the formation energy is in the range of the values published in the literature (∼200 meV/at. [11,44]).

(c) *Fe_3Al-$L1_2$*: We have studied $L1_2$ for comparison with the Fe_3AlC-$E2_1$ phase. Its lattice parameter and bulk modulus are found to be the same as Lechermann and Maugis [11,19]. $L1_2$ is slightly more stable than $D0_3$ (around 14 meV/at.), as recorded in previous studies (see in particular Ref. [19]), which is in contradiction with the experimental results [45]. This contradiction has been partially solved by Lechermann et al. [18] taking account the correlation effects (LDA + U approach). It is interesting to note that the difference in formation energies between ferro- and non-magnetic states is significant: around 400 meV/at. as Lechermann found [44]. We will see later that strong differences can also be noted on vibrational properties.

(d) *Fe_3AlC-$E2_1$*: The lattice parameter for κ-Fe_3AlC is greater than for $L1_2$ (around 3%), and corresponds well with the experimental value measured by Palm and Inden [8] (3.78 Å), or by Choo and [46] (3.74 Å). The occupation of the octahedral interstitial sites by the carbon atom induces an expansion of the lattice parameter (compared to $L1_2$), in agreement with intuition, which suggests that carbon insertion leads to a steric effect on the unit cell.

The formation energy, either in SGGA or in GGA, is smaller than proposed by Ohtani et al. [10] (−289.3 meV/at.), or obtained with the *VASP* package [11] (−188.2 meV/at.). The difference between our simulation and *VASP* simulation (around 50 meV/at.) can be attributed to the difference between pseudo-potential approaches (RRKJ versus PAW) [47]. Moreover, as our results on $D0_3$ and $L1_2$ systems are very close with those of Lechermann simulations [44], contrary once more to Ohtani, this suggests that the difference with Ohtani's results can probably be explained by the poorer convergence of their simulations [48].

The ferromagnetic and non-magnetic states of κ-Fe_3AlC have been investigated. The ground state is found 30 meV/at. in favor of the ferromagnetic state with a magnetic moment (1.1 μ_B/at.Fe) more than twice smaller than in Fe_3Al-$L1_2$ or $D0_3$. To understand why the magnetic moment decreases in comparison to the $L1_2$ system, we have evaluated the role of the lattice parameter on the magnetic moment. A numerical experience has been carried out, where the lattice parameter of κ (3.75 Å) has been imposed to Fe_3Al-$L1_2$. The results of this simulation ($\mu^{L1_2}(a_o = 3.75) = 2.35 > \mu^{L1_2}(a_o = 3.65) = 2.30$) show that the decrease of the magnetism from $L1_2$ to $E2_1$ is not due to the increase of the lattice parameter. We assume that it is only due to the interaction between iron and carbon atoms.

The bulk modulus of the κ phase is strongly increased both in SGGA (215 GPa) as in GGA (241 GPa) as compared to the $L1_2$ phase, indicating that carbon rigidifies the structure (see

Section 3.4), in relation to a strong interaction between carbon and iron atoms.

3.2. Fe_3Al-$L1_2$: electronic and vibrational properties

We now discuss the electronic and vibrational properties, and first those of the Fe_3Al-$L1_2$ phase. The electronic density of states (*e*DOS) and band structure within spin polarized approach are presented in Fig. 2 for the energy range $[-10; +5]$ eV, with respect to the Fermi level which is chosen to be zero (this convention has been conserved throughout this study). The band structure has been plotted along the high symmetry points of the cubic Brillouin zone.

The system exhibits a low density of states around the Fermi level, contrary to the κ phase. We have analyzed the electronic levels in terms of atomic orbital decompositions. Around $[-10; -5]$ eV the s states of the aluminium hybridize slightly with the s state of the iron, while around the Fermi level ($[-5; 0]$ eV) the p Al states hybridize with the d-Fe states.

We have then calculated within the SGGA and GGA approximations the vibrational band structure, and reported them in Fig. 3. In the case of the non-spin polarized approach (see dotted lines), we notice strong anomalies (''negative branches'' around **M** and **R** points) which reveal structural instabilities. This result indicates that Fe_3Al-$L1_2$ within a GGA approximation is not mechanically stable. On the contrary, within SGGA approach (thick lines), $L1_2$ is stable. Our simulations on Fe−Al systems reveal that the properties are very sensitive of the choice of the functional. For the following, we have decided to conserve SGGA results for $L1_2$.

We have plotted for information the total and projected (on non-equivalent atoms) vibrational density of states (see Fig. 3). As in the case of Fe_3Al-$D0_3$ or FeAl-B2 [49] the high frequency branches originate primarily from the low-mass Al atoms. These bands are separated by an optical gap from the low-frequency part which originates mainly from the high-mass Fe atoms. The range of frequencies is the same as for other Fe−Al ordered alloys. The width of the optical gap (around 0.7 THz) is the same as that found in the FeAl-B2 (see Fig. 4) or $D0_3$ systems [49]. Our results on Fe_3Al-$L1_2$ are qualitatively similar to those on Ni_3Al-$L1_2$ proposed by Iasev et al. [50].

The vibrational part of the free energy may change the relative stability between $L1_2$ and $D0_3$ compounds. In order to test this hypothesis, the vibrational free energy contributions of $L1_2$ and $D0_3$ have been calculated from the SGGA phonon spectra and Eq. (1). The vibrational properties of the $D0_3$ phase are not reproduced in the present paper, however, they have been calculated within the same approach, and compared successfully to the experimental data from Kentzinger et al. [53]. The vibrational free energies of $D0_3$ and $L1_2$ are reported in Fig. 5. At low temperature as at high temperature, assuming in first approximation that the lattice expansion can be neglected, the difference in F_{vib} is negligible (less 0.1 meV/at. at 1000 K). We conclude that the experimental stability of the $D0_3$ cannot be recovered from our results on vibrational part of the free energy.

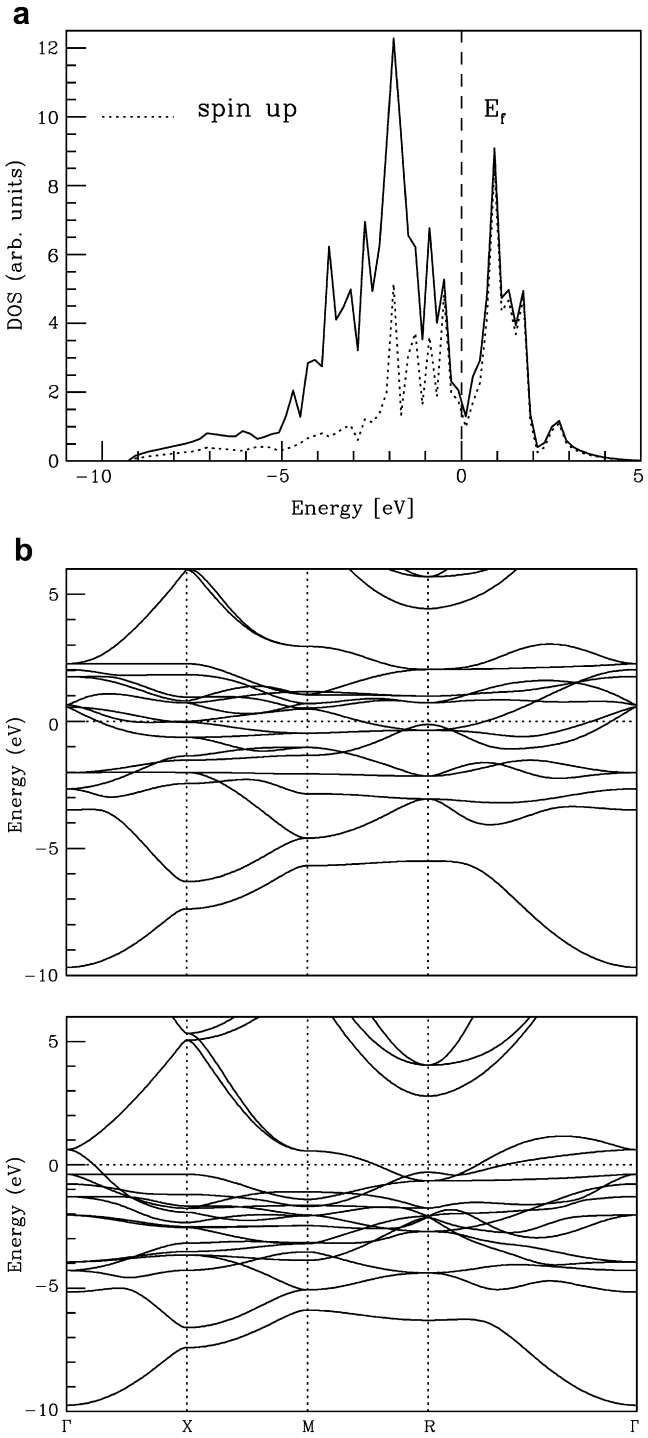

Fig. 2. Electronic density of states and band structure of Fe_3Al-$L1_2$: spin up (top) and down (bottom).

3.3. Fe_3AlC-$E2_1$: electronic and vibrational properties

We now examine the properties of the perovskite κ-Fe_3AlC. The *e*DOS and the electronic band structure have been drawn in Fig. 6, taking into account the spin effects.

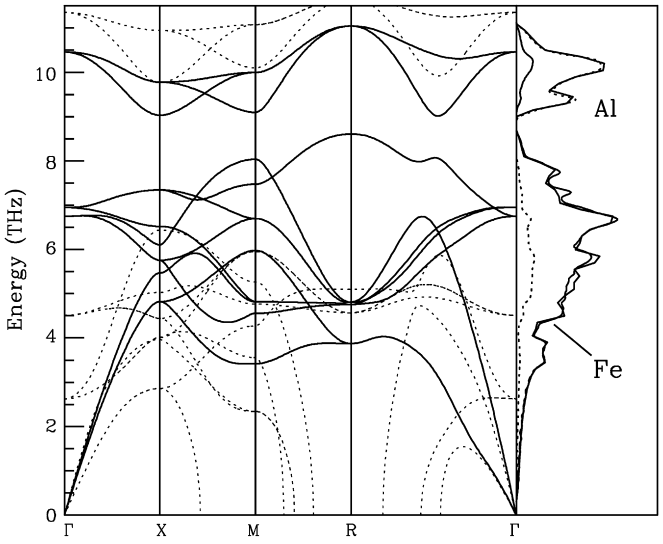

Fig. 3. On the left part of the figure, we have drawn the GGA (in dashed lines) and the SGGA (thick lines) vibrational band structure. On the right part of the figure we have plotted the total (thick lines) vibrational density of states of Fe_3Al-$L1_2$ within the only SGGA approach. We have added also for information the projected density of states on different non-equivalent atoms: iron contribution is in light lines while aluminium in dashed lines.

We notice that the carbon atom induces strong modification of the Fe_3Al-$L1_2$ electronic properties. The projected density of states in terms of atomic orbitals exhibits localized carbon states (see the main contributions reported in Fig. 6). In the range $[-14; -11]$ eV we identify essentially the s states of the carbon which are weakly hybridized with the iron s states. The p-C and the d-Fe states strongly hybridize around $[-7; -4]$ eV. This

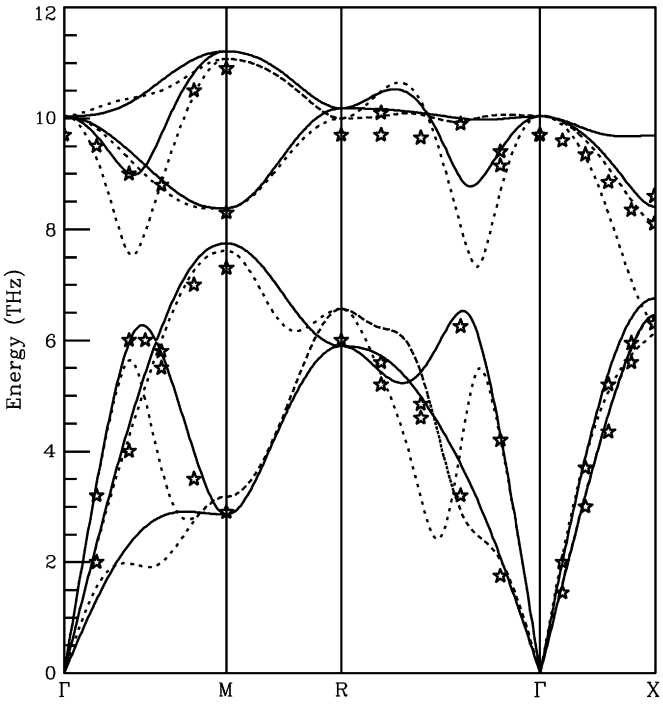

Fig. 4. Vibrational band structure of FeAl-B2, without spin effect in thick lines (without dashed lines). Experimental data are from Meyer et al. [49].

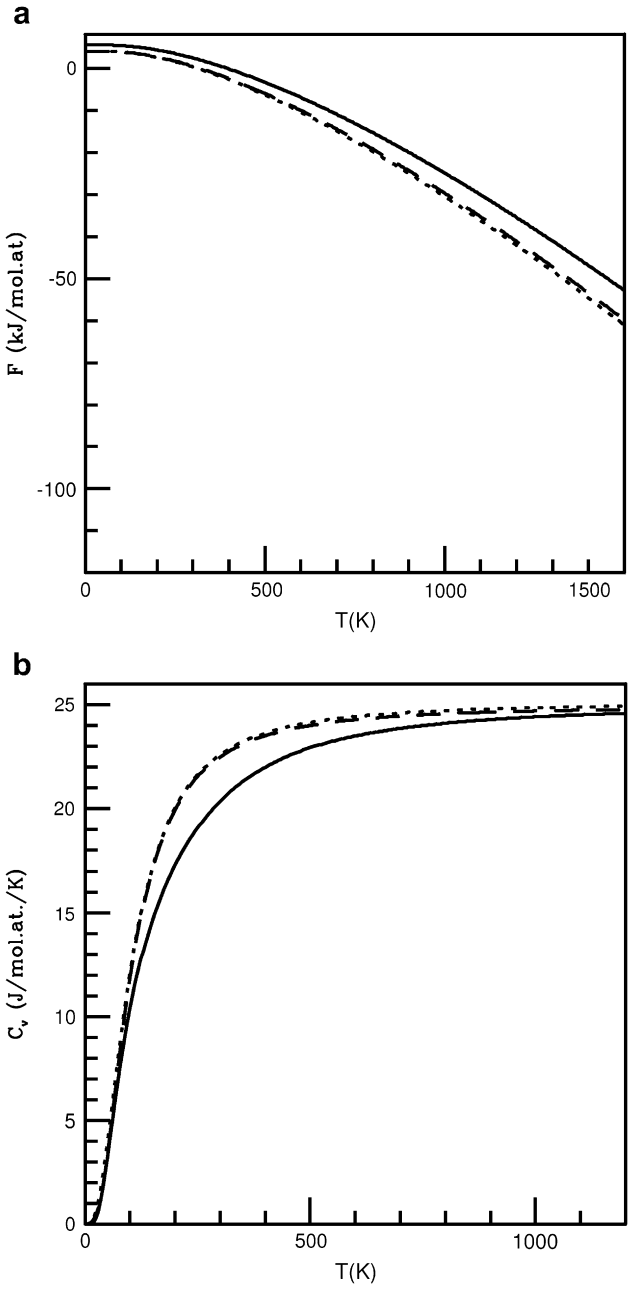

Fig. 5. Vibrational part of the free energy $F_{\rm vib}$ (in kJ/mol) and heat capacity C_v of the κ phase (solid line), of the Fe_3Al-$L1_2$ and $D0_3$ (in dashed and dotted lines), as a function of temperature.

hybridization can be interpreted by the ideal position of the iron atoms (along the $\{x; y; z\}$ axes), i.e. in the directions of the p-C orbitals.

In Fig. 7, we have plotted the vibrational band structure including (thick lines) or not (dotted lines) the spin effects, besides the total and projected vibrational density of states. We notice that, as for the electronic properties, the vibrational properties are modified by intercalation of carbon. Contrary to the $L1_2$ system, no strong differences can be noted here between GGA and SGGA functionals. Most of the differences can be attributed to the differences in lattice parameters: from

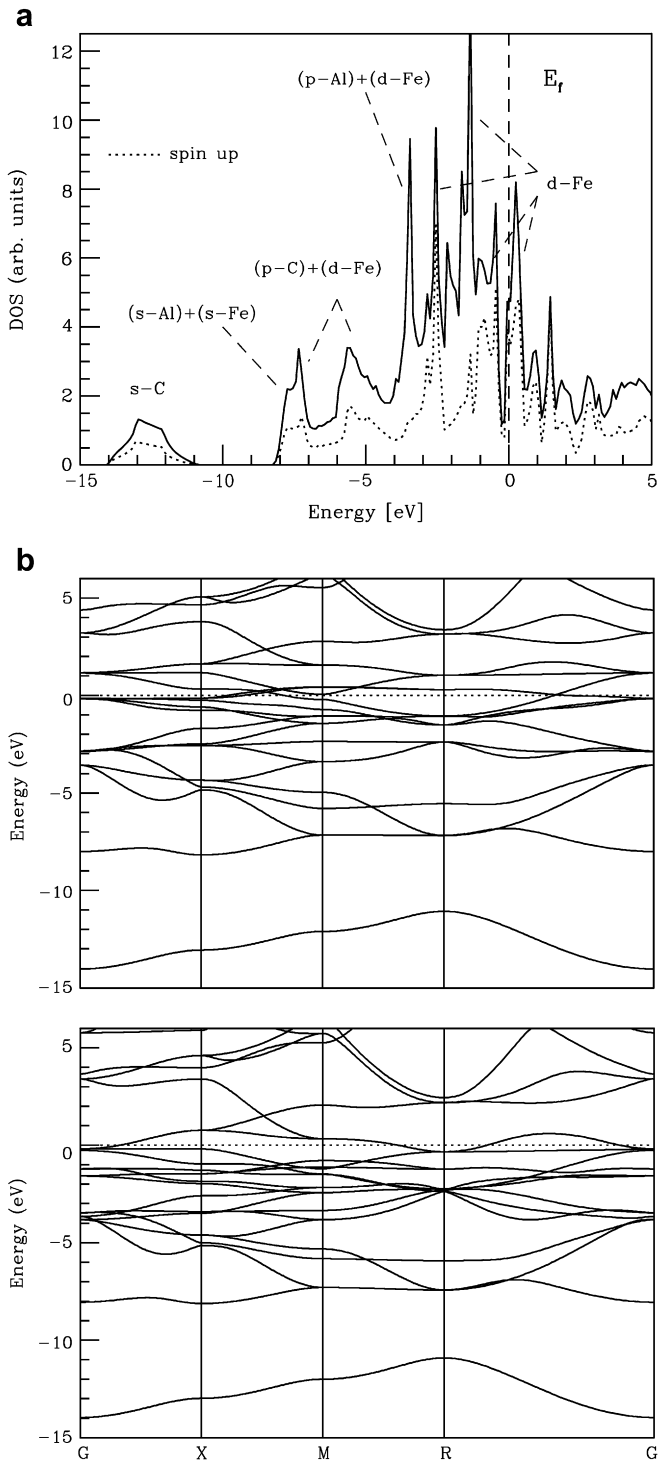

Fig. 6. Electronic density of states (left) and band structure of Fe_3AlC-$E2_1$: spin up (top) and down (bottom). On the *e*DOS we have written the main contribution states.

GGA to SGGA approach, the lattice parameter is increasing, thus inducing a decrease of the interatomic forces and hence of the frequencies. The main differences can be noticed on the acoustic modes around the Γ point (noted **G** in Fig. 7). They are related to strong modifications of the elastic constants (see Section 3.4).

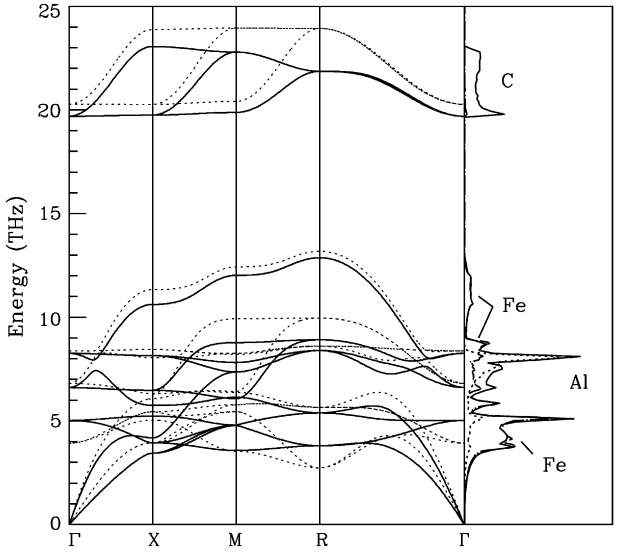

Fig. 7. Vibrational band structure and density of state of Fe_3AlC phase. See Fig. 3 concerning the convention used.

Moreover, in comparison to $L1_2$ (Fig. 3) the gap between aluminium and iron modes has disappeared, and we even find iron states above aluminium states. The carbon modes form a band at high energy (around 21 THz).

We have computed the vibrational part of the free energy and the heat capacity of the κ phase, and compared to those of Fe_3Al-$L1_2$ and $D0_3$. To evaluate the Debye temperature (q_D) we have fitted the theoretical C_v to the following formula [34]:

$$C_v = 9Nk_B\left(\frac{T}{\theta_D}\right)^3 \int_0^{\theta_D/T} \frac{x^4 e^x}{(e^x-1)^2}\mathrm{d}x \tag{3}$$

where N is the number of atoms. We find a Debye temperature equal to around 410 and 420 K for $D0_3$ and $L1_2$, respectively, while for κ we find 500 K. However, the Debye model does not reproduce correctly the heat capacity of the κ phase for the whole range of temperature (0−1500 K), contrary to the other Fe_3Al systems, especially at high temperature. The Debye model is indeed based on an acoustic/parabolic approximation, while in the case of κ, the optical modes of carbon induce strong deviations at high temperature.

3.4. Elastic constants

The elastic constants C_{ij} have been derived from the vibrational acoustic dispersion curves presented above. In the case of cubic systems, only three elastic constants are independent (see Ref. [34]): C_{11}, C_{12} and C_{44}. The slope of the acoustic branches (along the [100] direction) are directly related to C_{11} and C_{44}:

$$v_l^{[100]} = \sqrt{\frac{C_{11}}{\rho}} \text{ and } v_t^{[100]} = \sqrt{\frac{C_{44}}{\rho}} \tag{4}$$

Table 2
Calculated density of the unit cell (in kg/m^3) and elastic constants (in GPa) (experimental values are in parenthesis)

	ρ	C_{11}	C_{12}	C_{44}
C diamond	3490	1012 (1079 [34])	148 (124 [34])	529 (578 [34])
Al-fcc	2707	114 (114)	47 (62)	36 (32)
Fe-cc	7874	249 (233)	164 (135)	73 (117)
FeAl-B2	5839	270 (290 [52])	105 (130 [52])	152 (165 [52])
Fe_3Al-$D0_3$	6785	164 (171 [35])	127 (131 [35])	142 (132 [35])
Fe_3Al-$L1_2$	6612	184	145	160
Fe_3AlC-$E2_1$ (*sp*)	6527	453	100	69
Fe_3AlC-$E2_1$ (*np*)	6686	549	53	140

where $v_l^{[100]}$ and $v_t^{[100]}$ represent, respectively, the longitudinal and transverse velocity of sound in the compound and ρ, the density of the compound. For C_{12}, we have used the [111] direction:

$$v_l^{[111]} = \sqrt{\frac{C_{11} + 2C_{12} + 4C_{44}}{3\rho}} \tag{5}$$

There are other relations to evaluate the elastic constants, and we have verified that all relations are self-consistent.

Our results have been summarized in Table 2: the volume density and the elastic constants obtained for the reference phases, FeAl-B2, Fe_3Al-$D0_3$, Fe_3Al-$L1_2$ and Fe_3AlC-$E2_1$. In the case of structures not reported in this paper (Al-fcc, C diamond, Fe_3Al-$D0_3$ and Fe-bcc), we have checked that our vibrational properties are in good agreement with experimental data. In the case of the FeAl-B2 system, an approach without spin effects is necessary to calculate the vibrational properties. Indeed, SGGA simulations produce wrong results (see Fig. 4): note for example, that the gap disappears and some soft modes appear with SGGA, while GGA results can be fruitfully compared to the experimental data [49].

In the case of known systems the calculated elastic constants are in good agreement with experimental values (Table 2). For $L1_2$, the elastic constants are close to other Fe−Al systems, while for κ all elastic constants are greater, and in particular, C_{11} is more than three times higher than in other systems, which indicates that carbon strongly rigidifies the lattice.

From the set of elastic constants, practical parameters useful for a direct experimental comparison, such the bulk modulus B_o, the factor of anisotropy C_a, the shear modulus G, and the Young's modulus E along two crystallographic directions ([100], and [111]) can be calculated according to the relations:

$$\begin{cases} B_o = \frac{C_{11}+2C_{12}}{3} \\ C_a = \frac{C_{11}-C_{12}}{2C_{44}} \\ G = \frac{C_{11}-C_{12}}{2} \\ E_{100} = \frac{(C_{11}+2C_{12})(C_{11}-C_{12})}{C_{11}+C_{12}} \\ E_{111} = \left(\frac{1}{E_{100}} + \frac{C_{11}-C_{12}-2C_{44}}{3C_{44}(C_{11}-C_{12})}\right)^{-1} \end{cases} \tag{6}$$

For the systems for which the experimental values are known, our simulations give good results. In the case of the bulk modulus, we notice the agreement (around 10%) between the direct value via the Murnaghan's fit (see Table 1) and the results presented in Table 3, which proves the consistency of our approach.

The κ phase presents a large bulk modulus, and also a strong anisotropy ($C_a = 2.57/1.77$) in comparison to the other alloys. In usual cases of metals, C_a is smaller than 1, whereas for κ C_a is found greater than 1. This result is singular, and induces that E_{111} is smaller than E_{100}.

4. Conclusion

In conclusion, we have performed the first principle calculations of the Fe_3Al-$L1_2$ and the κ-Fe_3AlC structures. We have presented their structural, magnetic, electronic, vibrational and elastic properties. We have discussed about the magnetism, and the influence of the carbon on different properties of the system. As we show, the insertion of a carbon atom decreases the magnetism of the iron atoms, modifies strongly the heat capacity, and the elastic constants in κ as compared to Fe_3Al-$L1_2$. The interaction between Fe and C is the main origin of these modifications. In addition, in our comparison with Fe−Al systems, we have seen that the choice of the functional, and in particular the spin effects inside the *PBE* approximation, is delicate.

Table 3
Alternative set of elastic parameters: the bulk modulus B_o (in GPa), the factor of anisotropy C_a, the shear modulus G (in GPa), and the Young's modulus along two directions E_{100} and E_{111} (in GPa)

	B_o	C_a	G	E_{100}	E_{111}
C diamond	436	0.81	432 (478)	973 (1050)	1130 (1200)
Al-fcc	69	0.94	34	86 (64)	91 (76)
Fe-cc	181	0.63	47	131 (129)	197 (278)
FeAl-B2	160	0.54	82	211	346
Fe_3Al-$D0_3$	140	0.13	19	53	318
Fe_3Al-$L1_2$	158	0.12	19	55	358
Fe_3AlC-$E2_1$ (*sp*)	217	2.57	177	417	186
Fe_3AlC-$E2_1$ (*np*)	218	1.77	248	540	346

Acknowledgments

The authors acknowledge use of the supercomputer facilities at *Calmip* CICT Toulouse, France. Authors thank Pr. J. Morillo, R. Besson and A. Legris for fruitful discussions. D.C. acknowledges *Arcelor Research SA* for the funding.

References

[1] Sanders W, Sauthoff G. Intermetallics 1997;5:361;
Sanders W, Sauthoff G. Intermetallics 1997;5:377.
[2] Baligidad RG, Radhakrishna A. Materials Science and Engineering A 2001;308:136.
[3] Frommeyer G. Innovative steel research. Annual activity report. Max Planck Institute, Department of Materials technology; 2003. p. 19−20.
[4] Inoue A, Minemura T, Kitamura A, Masumoto T. Materials Transactions A 1981;12:1041.
[5] Chao C-Y, Liu CH. Materials Transactions 2002;43:2635.
[6] Li MC, Chang H, Kao PW, Gan D. Materials Chemistry and Physics 1999;59:96.
[7] Andryushchenko VA, Gavrilyuk VG, Nadutov VM. The Physics of Metals and Metallography 1985;60:50.
[8] Palm M, Inden G. Intermetallics 1995;3:443.
[9] Yang J, Laa P, Liu W, Hao Y. Materials Science and Engineering A 2004;382:8.
[10] Ohtani H, Yamano M, Hasebe M. ISIJ International 2004;44:1738.
[11] Maugis P, Lacaze J, Besson R, Morillo J. Metallurgical and Materials Transactions A 2006;37:3397.
[12] Morral FR. Journal of the Iron and Steel Institute 1934;130:419.
[13] Meyer L, Bühler H-E. Aluminium 1967;43:733.
[14] Krivonogov GS, Alekseyenko MF, Solovyeva GG. The Physics of Metals and Metallography 1976;39I:86.
[15] Parker SFH, Grundy PJ, Jones GA, Briggs I, Clegg AG. Journal of Materials Science 1988;23:217.
[16] The non-stoichiometric system will be presented in a following publication.
[17] Lechermann F, Fähnle M. Physical Review B 2001;63:012104.
[18] Lechermann F, Fähnle M, Meyer B, Elsasser C. Physical Review B 2004;69:165116.
[19] Lechermann F, Welsch F, Elsasser C, Ederer C, Fähnle M, Sanchez JM, et al. Physical Review B 2002;65:132104.
[20] Das GP, Rao BK, Jena P, Deevi SC. Physical Review B 2002;66:184203.
[21] Hohenberg P, Kohn W. Physical Review 1964;136:864.
[22] Kohn W, Sham L. Physical Review B 1965;140:1133.
[23] Perdew JP, Burke K, Ernzerhof M. Physical Review Letters 1996; 77:3865;
Perdew JP, Burke K, Ernzerhof M. Physical Review Letters 1997; 78:1396.
[24] S. Baroni, A. Dal Corso, S. de Gironcoli, P Giannozzi, C Cavazzoni, G Ballabio, et al. http://www.pwscf.org/.
[25] Vanderbilt D. Physical Review B 1990;41:7892.
[26] Rappe AM, Rabe KM, Kaxiras E, Joannopoulos JD. Physical Review B 1990;41:1227.
[27] Monkhorst HJ, Pack JD. Physical Review B 1976;13:5188.
[28] Murnaghan FD. Proceedings of the National Academy of Sciences of the United States of America 1944;30:244.
[29] Baroni S, Resta R. Physical Review B 1986;33:7017.
[30] Baroni S, Giannozzi P, Testa A. Physical Review Letters 1987;58:1861.
[31] Dal Corso A, de Gironcoli S. Physical Review B 2000;62:273.
[32] de Gironcoli S. Physical Review B 1995;51:6773.
[33] Favot F, Dal Corso A. Physical Review B 1999;60:11427.
[34] Kittel C. Solid state physics. New York: Wiley and Sons; 1976.
[35] Leamy HJ, Gibson ED, Kayser FX. Acta Metallurgica 1967;15:1827.
[36] Watson RE, Weinert M. Physical Review B 1998;58:5981.
[37] Moroni EG, Kresse G, Hafner J, Furthmüller J. Physical Review B 1997; 56:15629.
[38] Pickart SJ, Nathans R. Physical Review 1961;123:1163.
[39] Bogner J, Steiner W, Reissner M, Mohn P, Blaha P, Schwarz K, et al. Physical Review B 1998;58:14922.
[40] Pearson's Handbook Desk Edition. Crystallographic Data for Intermetallic Phases. P. Villars. Materials Park, OH: ASM International; 1997.
[41] Pearson WB. A handbook of lattice spacings and structures of metals and alloys. Oxford: Pergamon; 1958.
[42] Wakiyama T. Journal of the Physical Society of Japan 1972;32:1222.
[43] Palatnik LS, Tananko IA, Bobro YG. Kristallographiya 1964;9:163.
[44] Lechermann F, Fähnle M, Sanchez JM. Intermetallics 2005;13:1096.
[45] Binary alloy phase diagrams. 2nd ed. Materials Park, OH: ASM International; 1996.
[46] Choo WK, Han KH. Metallurgical Transactions A 1985;16A:5.
[47] We have increased strongly the cut-off energy and used a finest **k** mesh to verify the convergence of our simulations either with *VASP* either with *ESPRESSO* packages.
[48] We have verified the convergence of our results with higher convergence parameters: 100 Ryd and a $40 \times 40 \times 40$ **k** mesh.
[49] Meyer B, Schott V, Fähnle M. Physical Review B 1998;58:R14673.
[50] Isaev EI, Lichtenstein AI, Vekilov YuKh, Smirnova EA, Abrikosov IA, Simak SI, et al. Solid State Communications 2004;129:809.
[52] Fu CL, Yoo MH. Acta Metallurgica Materialia 1992;40:703.
[53] Kentzinger E, Cadeville MC, Pierron-Bohnes V, Petry W, Hennion B. Journal of Physics: Condensed Matter 1996;8:5535.